Electron-impact excitation of He-like ions: Mg XI

S. S. Tayal
Department of Physics and Astronomy, Louisiana State University, Baton Rouge, Louisiana 70803-4001
(Received 1 October 1986)

The collision strengths for the electron-impact excitation of inelastic transitions in Mg XI have been calculated by use of the R-matrix method. Eleven lowest LS target states $1s^2\,{}^1S$, $1s2s\,{}^{1,3}S$, $1s2p\,{}^{1,3}P^o$, $1s3s\,{}^{1,3}S$, $1s3p\,{}^{1,3}P^o$, and $1s3d\,{}^{1,3}D$ are included in the expansion of the total wave function. These target states are represented by accurate configuration-interaction wave functions. The lower partial-wave ($L \leq 8$) results obtained in the R-matrix method are supplemented by higher partial waves obtained in the close coupling with exchange terms omitted ($L = 9$—15), Coulomb-Born ($L = 16$—36), and Coulomb-Bethe ($L > 36$) approximations. Rydberg series of resonances converging to $n = 2$ and 3 thresholds are considered in the calculations. Results are obtained over a wide electron energy range (97.66—350.0 Ry) and are compared, where possible, with the previously available five-state Coulomb-exchange distorted-wave approximation results of Bednell. These collision strengths are then integrated with the assumption of a Maxwellian distribution of electron energies to obtain effective collision strengths for temperatures between 10^5 and 4×10^7 K.

I. INTRODUCTION

In recent years an enormous amount of observational data has become available from many satellite and rocket-borne experiments on solar plasmas. For example, the P78-1 and Solar Maximum Mission satellites[1,2] have provided a large amount of data for the most abundant of the ions of the helium isoelectronic sequence. Because of the large excitation and ionization energies, the ions of the helium sequence fall in the x-ray region of the spectrum and these ions tend to remain in the plasma for a longer time than the ions in other sequences. The ratio of the intensity of the forbidden line $1\,{}^1S$—$2\,{}^3S$ to the intercombination line $1\,{}^1S$—$2\,{}^3P^o$ provides a useful density diagnostic while the sum of the forbidden and intercombination lines to the resonance line $1\,{}^1S$—$2\,{}^1P^o$ gives a means of determining the temperature of the plasma.

The available experimental data on electron-impact excitation are very sparse, and one has to rely on theoretical calculations. Recently we have carried out accurate theoretical calculations[3–7] for electron-impact excitation of the He-like C V, O VII, and Mg XI ions using the R-matrix method.[8] In these calculations the lowest 11 LS target states, $1s^2\,{}^1S$, $1s2s\,{}^{1,3}S$, $1s2p\,{}^{1,3}P^o$, $1s3s\,{}^{1,3}S$, $1s3p\,{}^{1,3}P^o$, and $1s3d\,{}^{1,3}D$, were included in the R-matrix expansion. These target states were represented by accurate configuration-interaction (CI) wave functions. In our earlier calculations[7] on the Mg XI ion effective collision strengths for the spin-changing transitions among the target levels were reported. In this paper we extend our calculation on the Mg XI ion to the electric-dipole-allowed and forbidden transitions among the lowest 11 target states. The lower partial waves with angular momenta $L = 0$—8 were sufficient to give converged total collision for all the spin-changing transitions. However, for the transitions with associated dipole and quadrupole moments the higher partial waves make significant contributions to the total collision strengths. In order to obtain the converged collision strengths for these transitions for electron energies up to 350.0 Ry, the R-matrix results for lower partial waves ($L = 0$—8) are supplemented by higher-partial-wave results. The contribution from higher partial waves is obtained in the close-coupling approximation with exchange terms omitted and the Coulomb-Born approximation. The Coulomb-Bethe approximation is used to obtain partial contribution to the collision strength for higher partial waves ($L > 36$) in the high-energy region. Collision rates are obtained from collision strengths by integrating over a Maxwellian distribution of electron velocities.

The electron-impact excitation of the He-like ions has been studied previously by several authors. These earlier calculations include the Coulomb-Born calculations of Nakazaki[9] and Tully,[10] five-state close-coupling calculation of van Wyngaarden *et al.*[11] and the equivalent frozen-core approximation calculation of Bednell.[12] These calculations do not take resonance effects into account and give the nonresonant or background collision strengths. The importance of resonance effects for electron-impact excitation of He-like ions was examined in the recent R-matrix[3–7] and distorted-wave[13–15] calculations. These calculations show that the resonances make significant contributions to the collision strengths for many forbidden and intercombination transitions. However, the resonances are found to be less important for optically allowed transitions. Two independent five- and eleven-state R-matrix calculations[3,4] were carried out in our earlier work on C V and O VII ions in order to assess the relative importance of the Rydberg series of resonances converging to $n = 2$ and $n = 3$ complexes.

II. THE TARGET REPRESENTATION AND SCATTERING CALCULATIONS

The accuracy of the scattering calculations depends directly to first order on the accuracy of the target-state

wave functions. Eleven target eigenstates with configurations $1s^2\,{}^1S$, $1s2s\,{}^{1,3}S$, $1s2p\,{}^{1,3}P^\circ$, $1s3s\,{}^{1,3}S$, $1s3p\,{}^{1,3}P^\circ$, and $1s3d\,{}^{1,3}D$ are included in the expansion of the total wave function. These eigenstates are represented by CI wave functions constructed from eight orthogonal one-electron orbitals $1s$, $2s$, $2p$, $3s$, $3p$, $3d$ and pseudo-orbitals $4s$, $4p$. The $1s$ orbital is chosen to be hydrogenic and the other orbitals are obtained by optimizing the energy differences and oscillator strengths among the target states. The target wave functions used in the present calculations are described by Tayal and Kingston[7] where the orbital parameters, excitation energies and the oscillator strengths for the allowed transitions are listed. The agreement between the calculated and observed excitation energies is better than 1% for all the levels. There are 14 possible dipole-allowed transitions among 11 target states. For eight transitions the agreement between the length and velocity formulations of oscillator strengths is better than 1% while for other five transitions the agreement is 5% or better. The largest difference between the two forms of oscillator strength is for $1\,{}^1S-3\,{}^1P^\circ$ transition where it is about 6%.

In this work we are mostly concerned with electric-dipole-allowed and forbidden transitions which need higher-partial-wave contributions, particularly at higher energies. The scattering calculation can be divided in four parts depending on the partial wave range, as discussed before. The partial collision strengths for the lower partial waves ($L \leq 8$) has been calculated using the R-matrix method.[8] The R-matrix program package described by Berrington *et al.*[16] is used to calculate the $\underline{R}$ matrix on the boundary of a spherical region ($r_a = 4.0$ a.u.). We have included 25 continuum orbitals of each angular symmetry giving good convergence for energies up to 350.0 Ry. The number of bound three-electron configurations kept in the R-matrix expansion depends on the total angular momentum (L), spin (S), and parity (π). These configurations are generated by adding the third electron in all possible ways to all configurations that are included in the description of the target states, consistent with L, S, and π of the state. The calculations are carried out for doublet and quartet partial waves of both odd and even parities. The number of coupled channels for ${}^2S$ and ${}^2P^\circ$ partial waves are 11 and 17, respectively, while these are 19 each for ${}^2D$, ${}^2F^\circ$, ${}^2G$, and ${}^2H^\circ$.

In the outer region ($r > r_a$) where the exchange effects between the scattered electron and the target can be neglected, the coupled integrodifferential equations reduces to the set of n-coupled differential equations

$$\left[\frac{d^2}{dr^2}-\frac{l_i(l_i+1)}{r^2}+\frac{2Z}{r}+k_i^2\right]U_i(r) = 2\sum_{j=1}^{n} V_{ij}(r)U_j(r), \quad i=1,\ldots,n\ , \tag{1}$$

where

$$V_{ij}(r)=\frac{N}{r}\delta_{ij}+\mathrm{O}(r^{-2})\ . \tag{2}$$

Here we make a simplifying approximation by neglecting higher terms $\mathrm{O}(r^{-2})$ in Eq. (2) which reduces the coupled differential equations to the differential equation satisfied by Coulomb wave functions. It results in massive computer time savings, as the collision calculation in the outer region is carried out at large number of energy points in order to include explicitly the resonance structure in the cross sections. This approximation is not expected to introduce large errors in the collision strengths for the Mg ion considered in the present work, particularly for forbidden and intercombination transitions. However, the present results of collision strength for optically allowed transitions may be in error by approximately 5% because of this approximation.

The partial collision strengths for partial waves with angular momentum in the ranges $L = 9$–15 and $L = 16$–36 are calculated in the close-coupling approximation with exchange terms omitted using a noniterative integral equation method[17] and Coulomb-Born approximation, respectively. The same target wave functions are used in these calculations as in the R-matrix calculation. These partial waves are sufficient to give converged collision strengths for the forbidden transitions and some optically allowed transitions. However, for some other optically allowed transitions it is necessary to calculate the partial contribution to the collision strengths from higher partial waves with large angular momenta ($L \geq 37$). The Coulomb-Bethe approximation described by Burgess and Sheorey[18] is used to calculate the sum of partial collision strengths over higher partial waves for optically allowed transitions. The absorption oscillator strengths used in the Coulomb-Bethe calculations are tabulated by Tayal and Kingston.[7]

III. RESULTS AND DISCUSSION

A. Collision strengths

The collision strength for excitation from level i to level f is related to the cross section σ, in πa_0^2 units, by the following relation:

$$\Omega(i\rightarrow f)=\omega_i k_i^2\sigma(i\rightarrow f)\ , \tag{3}$$

where ω_i is the statistical weight of level i; k_i^2 is the energy in Ry of the electron relative to level i. The collision strengths are calculated over a wide range of incident electron energies (97.66–350.0 Ry). We have chosen a fine energy mesh for collision calculation in the threshold regions. This allowed us to delineate the resonance structure in the collision strengths which is expected to be important for low-energy electron scattering. At electron energies above 160.0 Ry the collision strengths for many transitions contained pseudoresonances which arise due to the inclusion of $4s$ and $4p$ pseudo-orbitals in the target wave functions. The smooth collision strengths within this region are obtained using a T-matrix smoothing procedure of Burke *et al.*[19] In this procedure the $\underline{T}$ matrices are calculated at a fine energy mesh covering the pseudo-resonance region with few energy points both above and below this energy region. Both the real and imaginary parts of the $\underline{T}$ matrices are energy averaged for each partial wave which are then used to obtain collision strengths.

In Table I we give the total collision strengths for the

TABLE I. Total collision strengths for inelastic transitions among $n=1$ and $n=2$ states. Numbers in square brackets denote power of ten.

Energy (Ry)	$1\,^1S-2\,^3S$	$1\,^1S-2\,^3P^\circ$	$1\,^1S-2\,^1S$	$1\,^1S-2\,^1P^\circ$	$2\,^3S-2\,^3P^\circ$	$2\,^3S-2\,^1S$	$2\,^3S-2\,^1P^\circ$	$2\,^3P^\circ-2\,^1S$	$2\,^3P^\circ-2\,^1P^\circ$	$2\,^1S-2\,^1P^\circ$
116.0	1.68[−3]	8.03[−3]	3.45[−3]	1.30[−2]	4.45	1.07[−2]	1.59[−2]	1.52[−2]	1.04[−1]	1.66
120.0	1.64[−3]	7.75[−3]	3.57[−3]	1.39[−2]	4.78	1.01[−2]	1.40[−2]	1.33[−2]	9.34[−2]	1.78
125.0	1.57[−3]	7.28[−3]	3.64[−3]	1.49[−2]	5.15	9.35[−3]	1.19[−2]	1.13[−2]	8.04[−2]	1.91
130.0	1.50[−3]	6.83[−3]	3.71[−3]	1.58[−2]	5.48	8.83[−3]	1.01[−2]	9.63[−3]	7.02[−2]	2.01
140.0	1.35[−3]	6.00[−3]	3.83[−3]	1.70[−2]	6.02	8.01[−3]	7.64[−3]	7.26[−3]	5.60[−2]	2.18
150.0	1.24[−3]	5.41[−3]	3.97[−3]	1.83[−2]	6.43	7.10[−3]	5.96[−3]	5.65[−3]	4.80[−2]	2.30
160.0	1.15[−3]	4.96[−3]	4.08[−3]	1.94[−2]	6.73	6.58[−3]	5.32[−3]	5.05[−3]	4.23[−2]	2.39
180.0	9.90[−4]	4.11[−3]	4.33[−3]	2.18[−2]	7.07	5.55[−3]	3.69[−3]	3.50[−3]	3.23[−2]	2.48
210.0	7.90[−4]	3.11[−3]	4.64[−3]	2.62[−2]	7.15	4.51[−3]	2.18[−3]	2.07[−3]	2.26[−2]	2.58
250.0	6.00[−4]	2.19[−3]	4.93[−3]	3.19[−2]	7.20	3.68[−3]	1.23[−3]	1.19[−3]	1.57[−2]	2.69
290.0	4.70[−4]	1.59[−3]	5.02[−3]	3.68[−2]	7.38	3.09[−3]	8.40[−4]	8.10[−4]	1.21[−2]	2.80
310.0	4.20[−4]	1.37[−3]	4.98[−3]	3.87[−2]	7.54	2.79[−3]	7.00[−4]	6.80[−4]	1.06[−2]	2.83
330.0	3.80[−4]	1.19[−3]	4.89[−3]	4.02[−2]	7.68	2.48[−3]	5.80[−4]	5.70[−4]	9.32[−3]	2.85
350.0	3.40[−4]	1.05[−3]	4.75[−3]	4.12[−2]	7.71	2.16[−3]	4.80[−4]	4.70[−4]	8.11[−3]	2.88

TABLE II. Total collision strengths for electron excitation of the $1s^2\,^1S$ and $1s2s\,^3S$ states to $n=3$ states. Numbers in square brackets denote power of ten.

Energy (Ry)	$1\,^1S-3\,^1S$	$1\,^1S-3\,^1D$	$1\,^1S-3\,^1P^\circ$	$2\,^3S-3\,^3S$	$2\,^3S-3\,^3P^\circ$	$2\,^3S-3\,^1S$	$2\,^3S-3\,^3D$	$2\,^3S-3\,^1D$	$2\,^3S-3\,^1P^\circ$
116.0	5.20[−4]	1.16[−4]	1.76[−3]	8.43[−2]	7.81[−2]	2.19[−3]	1.58[−1]	2.18[−2]	6.55[−3]
120.0	5.90[−4]	1.28[−4]	1.99[−3]	9.13[−2]	8.43[−2]	1.95[−3]	1.80[−1]	1.84[−2]	5.83[−3]
125.0	6.40[−4]	1.45[−4]	2.19[−3]	9.61[−2]	9.49[−2]	1.60[−3]	2.02[−1]	1.45[−2]	4.70[−3]
130.0	6.60[−4]	1.57[−4]	2.34[−3]	9.95[−2]	1.11[−1]	1.28[−3]	2.18[−1]	1.14[−2]	3.68[−3]
140.0	6.90[−4]	1.80[−4]	2.64[−3]	1.04[−1]	1.48[−1]	8.60[−4]	2.39[−1]	7.51[−3]	2.35[−3]
150.0	6.90[−4]	1.97[−4]	2.95[−3]	1.06[−1]	1.83[−1]	6.00[−4]	2.54[−1]	5.24[−3]	1.57[−3]
160.0	7.50[−4]	2.08[−4]	3.19[−3]	1.06[−1]	1.91[−1]	5.30[−4]	2.56[−1]	4.81[−3]	1.44[−3]
180.0	8.20[−4]	2.20[−4]	3.77[−3]	1.07[−1]	2.44[−1]	3.20[−4]	2.80[−1]	3.00[−3]	2.50[−3]
210.0	9.00[−4]	2.76[−4]	4.69[−3]	1.11[−1]	3.20[−1]	1.60[−4]	3.13[−1]	1.46[−3]	3.90[−3]
250.0	9.90[−4]	3.60[−4]	5.76[−3]	1.19[−1]	3.89[−1]	9.00[−5]	3.42[−1]	6.70[−4]	2.10[−3]
290.0	9.99[−4]	4.27[−4]	6.66[−3]	1.22[−1]	4.19[−1]	7.00[−5]	3.52[−1]	4.30[−4]	1.60[−3]
310.0	1.02[−3]	4.49[−4]	7.05[−3]	1.23[−1]	4.26[−1]	6.00[−5]	3.53[−1]	3.50[−4]	1.30[−3]
330.0	1.01[−3]	4.64[−4]	7.37[−3]	1.23[−1]	4.32[−1]	5.00[−5]	3.52[−1]	2.60[−4]	9.00[−4]
350.0	1.00[−3]	4.72[−4]	7.55[−3]	1.23[−1]	4.39[−1]	3.00[−5]	3.51[−1]	1.80[−4]	6.00[−4]

10 possible inelastic transitions among the $n=1$ and $n=2$ states, while Table II contains the total collision strengths for electron excitation of the ground $1\,^1S$ state and the first excited $2\,^3S$ state to the $n=3$ states at energies above the highest excitation threshold (116.0—350.0 Ry). The collision strengths for $1\,^1S-3\,^3S$, $-3\,^3P^\circ$, and $-3\,^3D$ transitions are not included in Table II, as these were reported in an earlier paper.[7] In this energy region the collision strengths vary smoothly with energy and show the expected large-energy behavior. The collision strengths for optically allowed transitions increase approximately, as $\ln E$, while for the spin-changing transitions they decrease rapidly with increasing energy. The collision strengths for the forbidden transitions such as $1\,^1S-3\,^1S$, $1\,^1S-3\,^1D$, $2\,^3S-3\,^3S$, $2\,^3S-3\,^3D$, etc., are approximately constant at high energies. The present results of collision strengths for the 10 inelastic transitions among the five $n=1$ and $n=2$ levels can be compared with the previously available values of Bednell[12] which he obtained in the five-state Coulomb exchange distorted-wave approximation. We have compared these results graphically in Figs. 1 and 2. His results are within 10—15% of the present values for all transitions but $2\,^3S-2\,^1S$ and $2\,^3P^\circ-2\,^1P^\circ$ in the energy range where his

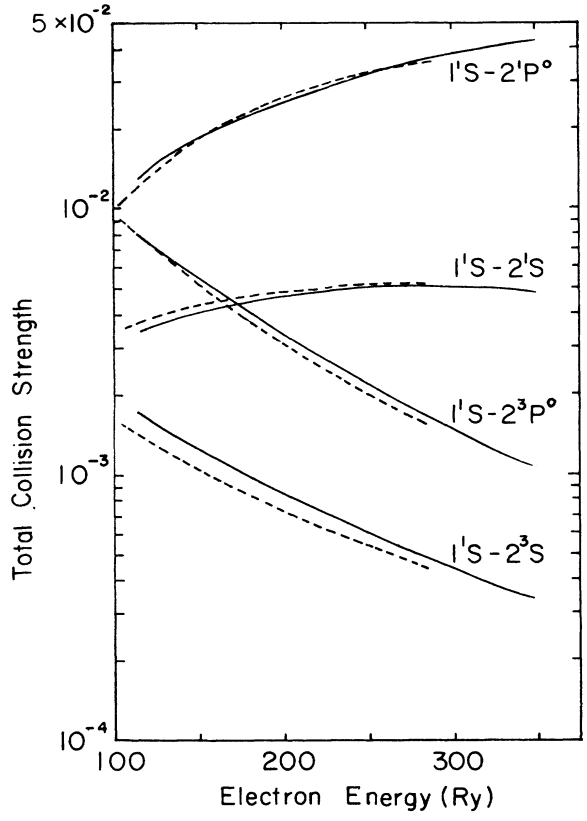

FIG. 1. Collision strengths for the electron excitation of ground $1\,^1S$ state to $n=2$ states in Mg XI as a function of electron energy in rydbergs. Solid curve, present eleven-state calculation; dashed curve, five-state Coulomb exchange distorted-wave results (Ref. 12).

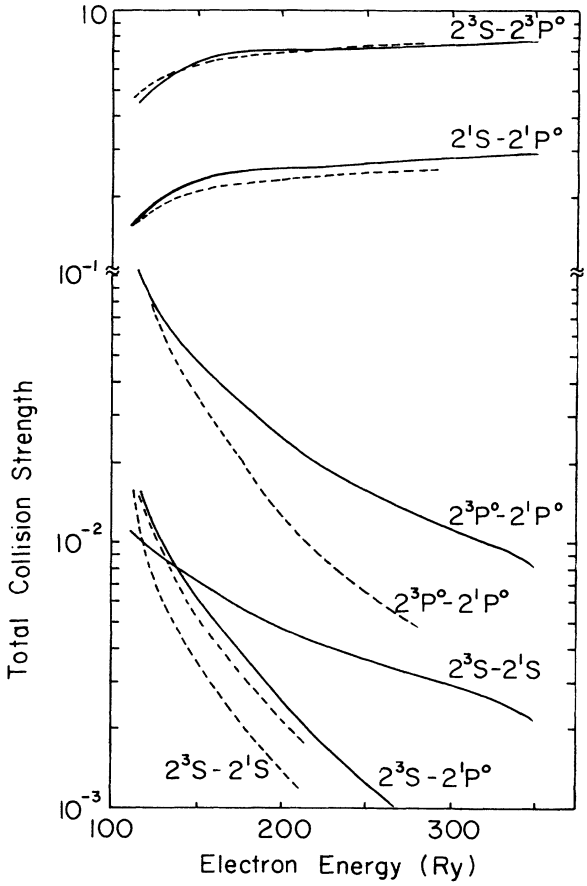

FIG. 2. The curves are the same as for Fig. 1, but for the transitions among $n=2$ levels in Mg XI.

results are available for comparison. For these two transitions the present results show slow fall off at high energies as compared to the Bednell[12] calculation. We have not shown the results for $2\,^3P^\circ-2\,^1S$ transition as these are approximately equal to that for $2\,^3S-2\,^1P^\circ$ transition. Pradhan *et al.*[13] also found that the collision strengths for $2\,^3S-2\,^1P^\circ$ and $2\,^3P^\circ-2\,^1S$ transitions are approximately

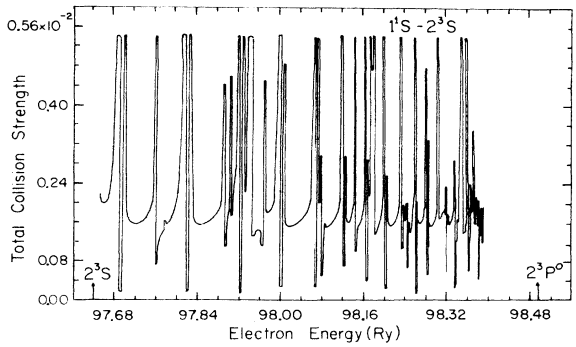

FIG. 3. Collision strength for the $1\,^1S-2\,^3S$ transition in Mg XI between the $2\,^3S$ and $2\,^3P^\circ$ thresholds.

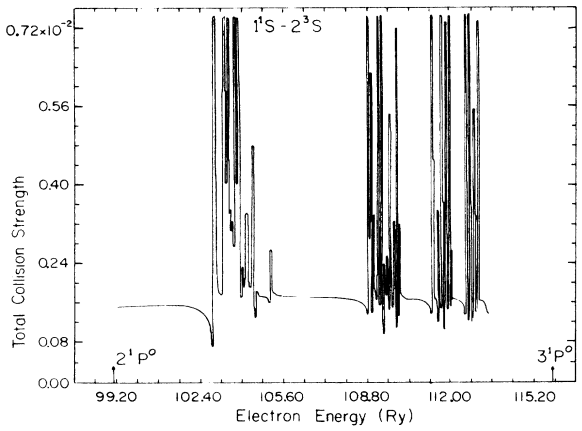

FIG. 4. Collision strength for the $1\,^1S-2\,^3S$ transition in Mg XI between $2\,^1P°$ and $3\,^1P°$ thresholds.

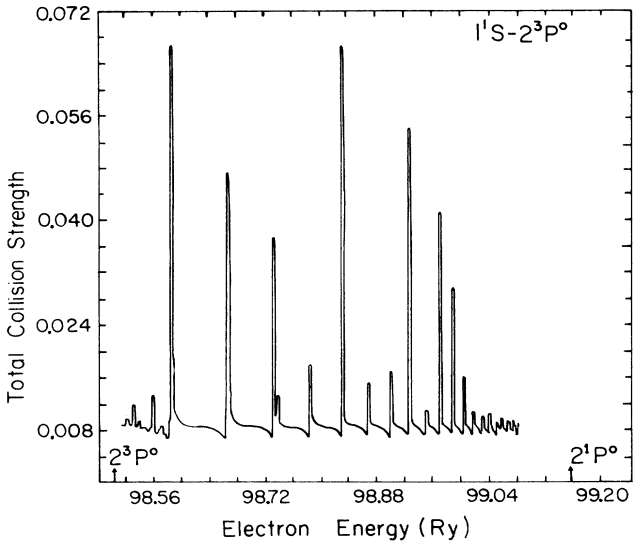

FIG. 5. Collision strength for the $1\,^1S-2\,^3P°$ transition in Mg XI between $2\,^3P°$ and $2\,^1P°$ thresholds.

equal for other ions of the helium sequence.

In the threshold regions we observe complicated series of resonances converging to different excitation thresholds of $n=2$ and $n=3$ complexes. In order to demonstrate the importance of Rydberg series of resonances at lower electron energies we give the total collision strength for $1\,^1S-2\,^3S$ transition between $2\,^3S$ and $2\,^3P°$, threshold in Fig. 3, while Fig. 4 gives the $1s\,3lnl'$ group of resonances for this transition. In Fig. 5 we have plotted the total collision strength for $1\,^1S-2\,^3P°$ transition between $2\,^3P°$ and $2\,^1P°$ thresholds. It is evident from these figures that the resonances are more important for $1\,^1S-2\,^3S$ transition than for $1\,^1S-2\,^3P°$ transition.

There are many partial waves contributing to these series of resonances. However, the dominant contribution comes from lower ^2S, $^2P°$, and ^2D partial waves which are important for the forbidden type of transitions. The resonances from higher partial waves are very narrow and do not contribute significantly to the total collision strengths. Therefore, the resonances are not expected to make appreciable contribution to the collision strengths for optically allowed transitions considered in the present work. A comparison of the resonance structures for the $1\,^1S-2\,^3S$ transition in Mg XI and C V[3] show that the resonance effects decrease with increasing nuclear charge.

B. Effective collision strengths

We are primarily concerned with calculating accurate electron excitation rates which can be compared with data

TABLE III. Effective collision strengths γ for Mg XI as a function of electron temperature. Numbers in square brackets denote power of ten.

	Electron temperature (10^5 K)									
Transition	1.0	4.0	8.0	10.0	20.0	50.0	80.0	100.0	200.0	400.0
$1\,^1S\rightarrow 2\,^1S$	5.93[−3]	4.11[−3]	3.81[−3]	3.76[−3]	3.69[−3]	3.80[−3]	3.95[−3]	4.05[−3]	4.37[−3]	4.68[−3]
$1\,^1S\rightarrow 3\,^1S$	6.42[−4]	5.74[−4]	5.90[−4]	5.99[−4]	6.31[−4]	6.80[−4]	7.20[−4]	7.49[−4]	8.53[−4]	9.19[−4]
$1\,^1S\rightarrow 2\,^1P°$	9.26[−3]	1.02[−2]	1.10[−2]	1.13[−2]	1.25[−2]	1.54[−2]	1.79[−2]	1.95[−2]	2.63[−2]	3.50[−2]
$1\,^1S\rightarrow 3\,^1P°$	2.05[−3]	1.91[−3]	2.00[−3]	2.05[−3]	2.26[−3]	2.84[−3]	3.36[−3]	3.68[−3]	4.99[−3]	6.68[−3]
$1\,^1S\rightarrow 3\,^1D$	1.53[−4]	1.29[−4]	1.34[−4]	1.37[−4]	1.50[−4]	1.81[−4]	2.11[−4]	2.30[−4]	3.12[−4]	4.12[−4]
$2\,^1S\rightarrow 3\,^1S$	4.37[−2]	3.42[−2]	3.37[−2]	3.39[−2]	3.50[−2]	3.69[−2]	3.82[−2]	3.89[−2]	4.18[−2]	4.59[−2]
$2\,^1S\rightarrow 2\,^1P°$	0.69	0.98	1.15	1.21	1.44	1.81	2.01	2.10	2.39	2.68
$2\,^1S\rightarrow 3\,^1P°$	2.74[−2]	2.54[−2]	2.81[−2]	2.99[−2]	3.98[−2]	6.50[−2]	8.24[−2]	9.10[−2]	1.15[−1]	1.31[−1]
$2\,^1S\rightarrow 3\,^1D$	5.20[−2]	5.05[−2]	5.47[−2]	5.66[−2]	6.47[−2]	7.97[−2]	8.90[−2]	9.38[−2]	1.10[−1]	1.26[−1]
$2\,^1P°\rightarrow 3\,^1S$	4.53[−2]	1.47[−2]	8.71[−3]	7.53[−3]	5.62[−3]	6.92[−3]	8.88[−3]	9.80[−3]	1.10[−2]	1.23[−2]
$2\,^1P°\rightarrow 3\,^1D$	2.02	0.71	0.53	0.51	0.49	0.61	0.70	0.74	0.75	0.78
$2\,^1P°\rightarrow 3\,^1P°$	0.12	0.11	0.11	0.11	0.12	0.12	0.13	0.13	0.14	0.14
$3\,^1S\rightarrow 3\,^1D$	4.24[−1]	3.78[−1]	3.77[−1]	3.78[−1]	3.81[−1]	3.85[−1]	3.85[−1]	3.84[−1]	3.82[−1]	3.79[−1]
$3\,^1S\rightarrow 3\,^1P°$	8.34	8.14	8.93	9.30	10.77	13.04	14.16	14.69	16.40	18.33
$3\,^1D\rightarrow 3\,^1P°$	13.56	13.35	14.78	15.44	17.98	21.66	23.36	24.13	26.61	29.52

TABLE IV. Effective collision strengths γ for Mg XI as a function of electron temperature.

Transition	Electron temperature (10^5 K) 1.0	4.0	8.0	10.0	20.0	50.0	80.0	100.0	200.0	400.0
$2\,^3S\rightarrow 2\,^3P^\circ$	1.83	2.51	3.00	3.17	3.82	4.90	5.48	5.75	6.52	7.33
$2\,^3S\rightarrow 3\,^3S$	0.16	0.11	0.10	0.099	0.10	0.10	0.11	0.11	0.11	0.11
$2\,^3S\rightarrow 3\,^3P^\circ$	0.092	0.084	0.088	0.092	0.11	0.16	0.20	0.23	0.31	0.41
$2\,^3S\rightarrow 3\,^3D$	0.19	0.17	0.18	0.18	0.20	0.23	0.25	0.26	0.29	0.30
$2\,^3P^\circ\rightarrow 3\,^3S$	0.057	0.041	0.037	0.037	0.031	0.031	0.035	0.037	0.049	0.064
$2\,^3P^\circ\rightarrow 3\,^3P^\circ$	0.43	0.37	0.36	0.36	0.36	0.37	0.37	0.37	0.36	0.35
$2\,^3P^\circ\rightarrow 3\,^3D$	1.36	1.24	1.27	1.30	1.44	1.77	2.04	2.19	2.75	3.34
$3\,^3S\rightarrow 3\,^3P^\circ$	23.01	22.79	24.76	25.71	29.64	36.21	39.57	41.12	46.04	51.62
$3\,^3S\rightarrow 3\,^3D$	1.45	1.28	1.26	1.25	1.24	1.21	1.19	1.19	1.18	1.17
$3\,^3P^\circ\rightarrow 3\,^3D$	36.36	35.06	37.91	39.29	45.01	54.51	59.25	61.36	67.70	74.24

for laboratory and astrophysical plasmas. When the plasma is in ionization equilibrium the temperature for the maximum abundance of Mg XI ion is approximately 4×10^6 K. It is convenient to define the effective collision strength

$$\gamma(i\rightarrow f)=\int_0^\infty \Omega(i\rightarrow f)\exp(-E_f/kT_e)d(E_f/kT_e)\ , \qquad (4)$$

where E_f is the energy of the incident electron with respect to the upper level f, T_e is the electron temperature in K, and k is Boltzmann constant. The excitation $q(i\rightarrow f)$ and deexcitation $q(f\rightarrow i)$ rate coefficients are given by

$$q(i\rightarrow f)=\frac{\omega_f}{\omega_i}q(f\rightarrow i)\exp(-E_{if}/kT_e)\ (\mathrm{cm^3\,s^{-1}}) \qquad (5)$$

and

$$q(f\rightarrow i)=\frac{8.63\times 10^{-6}}{\omega_f T_e^{1/2}}\gamma(i\rightarrow f)\ (\mathrm{cm^3\,s^{-1}})\ , \qquad (6)$$

where ω_i and ω_f are the statistical weights of the levels i and f.

The effective collision strengths obtained from the collision strengths by integrating over a Maxwell velocity distribution are tabulated in Tables III and IV for 10 temperatures (1×10^5–4×10^7 K) covering the range of maximum abundance of Mg XI ions under the conditions of ionization equilibrium. Tables III and IV give the results for transitions among the levels with multiplicity equal to one and three, respectively. The effective collision strengths for the transitions of the type $n\,^1S$–$n'\,^1S$ first decrease and then increase with the increase in temperature. The effective collision strengths are larger at lower temperatures because of the presence of resonances in the total collision strengths at low electron energies. Similar situations arise for the forbidden transitions from $n\,^1S$ states to the $3\,^1D$ state. The resonance contributions for these transitions are much less important than for the forbidden $1\,^1S$–$2\,^3S$ transition. The effective collision strengths for the dipole-allowed $n\,^1S$–$n'\,^1P^\circ$ and $n\,^3S$–$n'\,^3P^\circ$ transitions generally increase with the increase in temperature over the entire temperature range. Our results of γ for the transitions with $3\,^1P^\circ$ as upper level may be slightly in error at lower temperatures. The effective collision strengths γ for the forbidden $2\,^1P^\circ$–$3\,^1P^\circ$, $n\,^3S$–$n'\,^3D$, and $n\,^3S$–$n'\,^3S$ transitions remain approximately constant with temperature, while γ for the transitions $2\,^1P^\circ$–$3\,^1S$, $-3\,^1D$ and $2\,^3P^\circ$–$3\,^3S$, $-3\,^3P^\circ$ show decreasing trend first and then increase with increasing temperatures.

IV. CONCLUSION

In this paper we have presented collision strengths and effective collision strengths for several transitions obtained using the R-matrix method for lower partial waves ($L\leq 8$) and close coupling with the omission of exchange terms ($9\leq L\leq 15$), Coulomb-Born ($16\leq L\leq 36$), and Coulomb-Bethe ($L=37-\infty$) for higher partial waves. Accurate CI wave functions are used for the target representation. We have investigated the resonance structure below the $n=2$ and $n=3$ levels. In the present calculations it is assumed that the magnetic interactions are negligible and the total orbital and total spin angular momenta are separately conserved and also the radiative decay of the resonant states has been ignored. The present results may be in slight error for some transitions because of these assumptions. We have also ignored the long-range potential coefficients in the evaluation of coupled differential equations in the outer region which may cause an error of up to 5% for the dipole allowed transitions.

ACKNOWLEDGMENTS

The author would like to thank Dr. Ronald J. W. Henry for his help and encouragement. This work is supported in part by the Department of Energy, Office of Basic Energy Sciences.

[1]D. L. McKenzie and P. B. Landecker, Astrophys. J. **259**, 372 (1982).
[2]D. L. McKenzie, R. M. Broussard, P. B. Landecker, H. R. Rugge, R. M. Young, G. A. Doschek, and U. Feldman, Astrophys. J. **238**, L43 (1980).
[3]S. S. Tayal, Phys. Rev. A **34**, 1847 (1986).
[4]A. E. Kingston and S. S. Tayal, J. Phys. B **16**, 3465 (1983).
[5]S. S. Tayal and A. E. Kingston, J. Phys. B **17**, L145 (1984).
[6]S. S. Tayal and A. E. Kingston, J. Phys. B **17**, 1383 (1984).
[7]S. S. Tayal and A. E. Kingston, J. Phys. B **18**, 2983 (1985).
[8]P. G. Burke and W. D. Robb, Adv. At. Mol. Phys. **11**, 143 (1975).
[9]S. Nakazaki, J. Phys. Soc. Jpn. **41**, 2084 (1976).
[10]J. A. Tully, J. Phys. B **7**, 386 (1974).
[11]W. L. Wyngaarden, K. Bhadra, and R. J. W. Henry, Phys. Rev. A **20**, 1409 (1979).
[12]N. R. Bednell, J. Phys. B **18**, 955 (1985).
[13]A. K. Pradhan, D. W. Norcross, and D. G. Hummer, Phys. Rev. A **23**, 619 (1981).
[14]A. K. Pradhan, Phys. Rev. A **28**, 2128 (1983).
[15]L. Steenman-Clark and P. Fancher, J. Phys. B **17**, 73 (1984).
[16]K. A. Berrington, P. G. Burke, M. Le Dourneuf, W. D. Robb, K. T. Taylor, and Vo Ky Lan, Comput. Phys. Commun. **14**, 367 (1978).
[17]R. J. W. Henry, S. P. Rountree, and E. R. Smith, Comput. Phys. Commun. **23**, 233 (1981).
[18]A. Burgess and V. B. Sheorey, J. Phys. B **7**, 2403 (1974).
[19]P. G. Burke, K. A. Berrington, and C. V. Sukumar, J. Phys. B **14**, 289 (1981).